Design of a compact serial-kinematic scanner for high-speed atomic force microscopy: an analytical approach

S.P. Wadikhaye, Y.K. Yong, S.O.R. Moheimani

School of Electrical Engineering and Computer Science, The University of Newcastle, Callaghan 2308, NSW, Australia
E-mail: sachin.wadikhaye@uon.edu.au

Published in Micro & Nano Letters; Received on 9th September 2011; Revised on 7th December 2011

A systematic procedure for designing a high-speed, compact serial-kinematic XYZ scanner for atomic force microscopy is presented in this Letter. Analytical stiffness calculations are used to estimate the first natural frequency and travel range of the scanner. Design and characterisation of the scanner are presented. Results of finite-element analysis and experimentation on the scanner revealed natural frequencies of 10, 7.5 and 64 kHz for X, Y and Z stages, respectively. Maximum travel range of 8, 6 and 2 μm were measured along x, y and z directions. Performance evaluations were conducted by implementing the scanner in a commercial atomic force microscope. Images of a 6 × 4.5 μm area of a calibration grating were captured at line rates of 10, 50, 78, 100, 120 and 150 Hz with 256 × 256 pixel resolution. Limitations in design and suggestions for improvement of the scanner performance are discussed.

1. Introduction: In 1986, Binnig and Quate [1] introduced the first atomic force microscope (AFM) to scan any surface with nanometre accuracy. Since the invention, AFMs have been one of the most versatile characterisation and manipulation devices in the field of nanotechnology. In recent years, applications of AFM have been growing and researchers in many fields are attempting to customise AFMs as per their requirements [2, 3]. High-speed AFM is one such requirement which enables researchers to visualise biological processes, such as protein interaction [2] which occur in milliseconds or less. A high-speed AFM scanner is a critical component for a high-speed AFM. Scanners installed in most of the commercial AFMs are piezoelectric tube scanners. They have a low natural frequency which typically limits the scanning speed of the AFM to a few Hertz [4]. Another class of scanners which are seen as alternatives to piezoelectric tube scanners for high-speed scanning are the flexure-based scanners [5].

Most of the commercial AFMs are equipped with compact piezoelectric tube scanners. To design a compact flexure-based scanner that would replace an existing piezoelectric tube scanner in a commercial AFM is a difficult task. Manufacturing constraints and machining tolerances imposed on the design (such as the smallest available tool in the market) make the design process for a compact scanner even more challenging. There has been more effort put forward to generalise the design process using finite-element analysis (FEA) [6], which is an iterative approach. A more systematic procedure is needed for the design of a scanner to overcome the space and manufacturing constraints.

Flexure hinges have been used extensively in designing AFM scanners as they provide smooth motions through elastic deformation [7]. Nonlinearities such as friction and backlash can be avoided by using flexure hinges. Analytical models for flexure hinges proposed in the literature can be used to determine the stiffness of flexure hinges [8–10]. These analytical models are based on the strain energy approach and Castigliano's displacement theorem. Force–displacement relationship can be derived from these models and thus stiffness of hinges can be calculated. An approach to calculate the stiffness of a double-hinged flexure with corner-fillet hinges is given in [11]. The same approach is applied to calculate the stiffness of the double-hinged flexure with right circular hinges, for the design of the nanopositioning scanner, in this Letter.

In this Letter, an analytical procedure for designing a high-speed, compact serial-kinematic AFM scanner is presented. An advantage of a serial-kinematic scanner is that each axis can be modelled as a single degree-of-freedom (SDOF) mass-spring system. There is a trade-off between the natural frequency and the travel range of the stage. It is shown in this Letter that the stiffness of the structure is the key parameter to reach a break even. The use of analytical stiffness calculations for the double-hinged flexure with right circular hinges makes the design process more systematic and parametric. The design process is effectively reduced for the selection of two parameters of the double-hinged flexure, while the rest of the parameters are dictated by space constraints. The choice of these two parameters determines the stiffness value which can achieve a compromise between natural frequency and range of motion.

2. Design: One characteristic of serial-kinematic flexure-based nanopositioners is that they can be designed as a mass-spring system. Each stage (X, Y or Z stage) can be considered as a separate mass-spring system with flexures modelled as springs. The natural frequency of a SDOF spring-mass system is $\omega_n = \sqrt{k/m}$, which shows that, for a constant mass m, natural frequency ω_n varies as the square root of stiffness k. Based on this fact, the natural frequency of the nanopositioning stage can be optimised by varying its stiffness. To obtain high scanning rate while maintaining planar motion, the lateral stiffness K_{yy} (along the axis of actuation) and the out-of-plane stiffness K_{zz} play major roles. Stiffness of flexure can be derived using the Castigliaono's displacement theorem [12].

Consider a beam with rectangular cross-section and constant thickness t as shown in Fig. 1*a*. A point load F_y is applied in the y-direction at one end while keeping the other end fixed. The

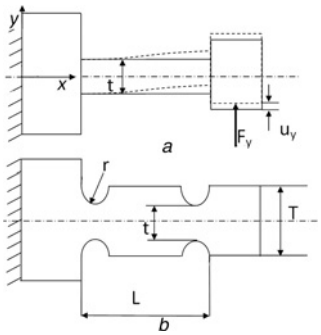

Figure 1 *Top view of the flexures shows the variation in thickness*
a Generic rectangular compliant beam
b Double-hinged flexure with right circular hinges

total strain energy for bending is given as:

$$U = \int_0^L \frac{M^2\,\mathrm{d}x}{2EI(x)} + \int_0^L \frac{\alpha V\,\mathrm{d}x}{2GA(x)} \tag{1}$$

For a beam with rectangular cross-section, cross-sectional area $A(x)$ and moment of inertia $I(x)$ are constant, as the thickness is constant. But for the case of double-hinged flexures, t is varied along the x-direction as shown in Fig. 1*b*. The equation for calculating thickness $t(x)$ for double-hinged flexure with corner-fillet hinges is given in [11]. This approach is extended to derive the variation in thickness $t(x)$ for double-hinged flexures with right circular hinges as

$$t(x) = \begin{cases} t + 2[r - \sqrt{x(2r-x)}], & \text{if } x \in [0, m] \\ t + 2[r - \sqrt{(j)(2r-j)}], & \text{if } x \in [m, n] \\ t + 2r, & \text{if } x \in [n, o] \\ t + 2[r - \sqrt{(k)(2r-k)}], & \text{if } x \in [0, p] \\ t + 2[r - \sqrt{(g)(2r-g)}], & \text{if } x \in [0, m] \end{cases} \tag{2}$$

where $m = r$, $n = 1 = 2r$, $o = L - l = L - 2r$, $p = L - r$, $j = l - x$, $k = l - g$ and $g = L - x$.

Thus, $A = ht(x)$ and $I = ht(x)^3/12$, which are substituted in (1) give:

$$U = \int_0^L \frac{M(x)^2\,\mathrm{d}x}{2E[ht(x)^3]/12} + \int_0^L \frac{\alpha V(x)\,\mathrm{d}x}{2Ght(x)} \tag{3}$$

By substituting bending moment $M(x) = F_y x$ and shear force $V = F_y$ into (3) and taking partial derivative with respect to F_y yields the deflection of beam along y-direction as:

$$u_y = \frac{\partial U}{\partial F_y} = \frac{12F_y}{Eh}\int_0^L \frac{x^2}{t(x)^3}\,\mathrm{d}x + \frac{\alpha F_y}{Gh}\int_0^L \frac{1}{2t(x)}\,\mathrm{d}x \tag{4}$$

A similar approach can be adopted to derive u_z. The stiffness can be evaluated using $K_{ij} = F_i/u_j$.

A step-by-step procedure for designing the lateral stages of a serial-kinematic scanner is presented below:

1. Determine the suitable stiffness of the stage K_s to satisfy the required natural frequency and range of motion. The natural frequency is given by:

$$f_n = \frac{1}{2\pi}\sqrt{\frac{K_s}{m}} \tag{5}$$

The range can be estimated from

$$\Delta L = \frac{K_{\text{piezo}}}{K_s + K_{\text{piezo}}}\Delta L_o \tag{6}$$

where f_n is the natural frequency of the stage in Hz, m is the mass of the stage, K_{piezo} is the stiffness of the piezoelectric stack actuator, ΔL_0 is the maximum elongation of a piezoelectric stack actuator and ΔL is the achievable range [13].

2. Determine the number of flexures that can be accommodated to the designated space. Determine the stiffness of each flexure, K_{flex}, by dividing the stiffness of the stage K_s by the number of flexures.
3. From the stiffness derivation, a table for the stiffness K_{yy} and K_{zz} is generated for different combinations of radius r and thickness t. Suitable t and r values of the flexures are selected from the table to obtain the required stiffness K_{flex}.

The design of a compact high-speed scanner, based on the above procedure, is presented here. The aim is to replace the commercial piezoelectric tube scanner of an NT-MDT NTEGRA AFM. A serial-kinematic configuration is used where the Y-stage accommodates the X-stage, whereas the Z-stage is encompassed in the X-stage. The design should be able to fit in a 45 mm diameter space, with fast stage having a natural frequency of 20 kHz along the direction of actuation and maximum displacement of the lateral stages should be at least 10 μm.

As mentioned, each stage can be approximated as a separate spring-mass system. The design of the fast stage is presented as an illustration to understand the design process. The X-stage was estimated to have an effective mass of 2.28 g. The unloaded range of motion for the piezoelectric stack actuators ΔL_0 as per manufacturer was 11.3 μm with stiffness 84.75 N/μm. Following the Step 1 of the procedure, to achieve a natural frequency of 6.6 kHz (without taking the actuator into consideration), for the stage with a travel range of 10.75 μm, the stiffness of the structure K_s was estimated to be 4 N/μm. The height h and the length L of the flexures are limited by the space constrained to 12.8 and 5.3 mm, respectively, due to the space constraint. The X-stage encompasses the Z-stage; hence, the dimensions of the X-stage were estimated to be 8 × 8 mm, to accommodate the Z-stage piezoelectric stack. The number of flexure members that can be placed in an 8 mm length stage with reasonable manufacturing clearance was found to be three. So, every flexure should be designed to have stiffness of approximately 1.33 N/μm to obtain a structural stiffness of 4 N/μm.

Following Step 3 of the procedure, t and r are varied from 0.2 to 0.7 mm with different t/r ratios. For $t = 0.4$ mm and $r = 0.45$ mm, stiffness $K_{yy} = 1.354$ N/μm and $K_{zz} = 12.98$ N/μm were found, which satisfy the scanner design specifications. The Y-stage (slow stage) was designed following the same procedure and the design parameters t and r were both found to be 0.4 mm to obtain natural frequency of 7.5 kHz and range of 10.5 μm.

Aluminium alloy 7075 was used for manufacturing the scanner. For high-precision manufacturing of the scanner wire-electrical-discharge-machining technique was used. A base, which is used to mount the scanner to the arrangement provided for the piezoelectric tube scanner, was manufactured in-house. Ports were provided on the scanner for mounting capacitive sensors and piezoelectric stack actuators. For high acceleration actuation of the stage along x and y directions, piezoelectric stack actuators from Noliac (SCMAP07, 5 × 5 × 10 mm, 380 nF) were used. For actuation along the z-direction, a Noliac (SCMAP06, 3 × 3 × 4 mm, 35 nF) actuator was used. These actuators were driven by three external voltage amplifiers PiezoDrive PDL 200 with gain of 20. Displacement sensing was accomplished using ADE technologies 8810/2804 capacitive sensors with a gain of 2.5 μm/V.

High-speed scanning is not possible using the NT-MDT NTEGRA SPM data acquisition system. Its sampling rate limits the scanning speed to 31 Hz for acquiring an image of 256 × 256 pixel resolution. An increased scan rate of 62 Hz can be achieved at the cost of image quality by reducing the resolution to 128 × 128 pixel. To achieve higher line rates, a dSPACE-1103 rapid prototyping system is used, which increases the scanning rate to 80 kHz. A line rate of 155 Hz can be achieved with a 256 × 256 pixel resolution. Higher line rates of 200 Hz with a 200 × 200 pixel resolution can be achieved by using this prototyping system.

3. FEA of the scanner: ANSYS was used to perform static stress analysis to find out high stress points for a 10 μm displacement of X and Y stages. It was found that the stresses in the system did not exceed the acceptable stress limit. Extra material was removed from the low stress points, causing an increase in the natural frequency of the system. Bolt positions were finalised to avoid high stress points and to provide rigidity to the structure. Thus, design configuration of the scanner was finalised. Modal analysis was carried out to identify the resonant modes of the scanner assembly. The predictions from FEA were later compared with the analytical and experimental results to evaluate the

doi: 10.1049/mnl.2011.0477

Table 1 Material properties for FEA

Material	E, GPa	ρ, g/cm	ν
Aluminium alloy	72	2.81	0.33
Steel	200	7.8	0.28
Piezoelectric stack	33.9	8.0	–

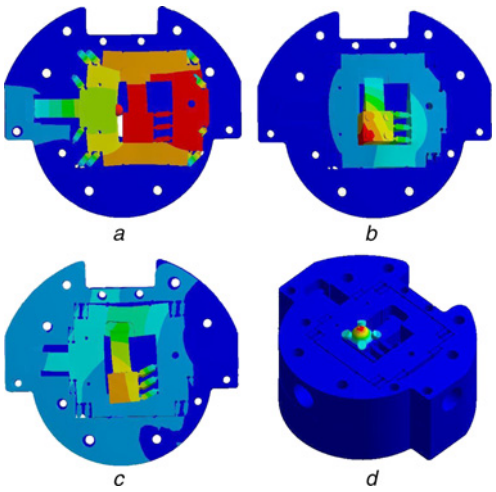

Figure 2 *Results of modal analysis conducted on the scanner*
a First resonance appears along the *Y*-axis at 7.67 kHz
b Second resonance is the rocking mode on the X-stage at 10.26 kHz
c Third resonance is observed along the *x*-direction at 16.4 kHz
d Resonance frequency of the Z-stage is at 115.4 kHz

applicability of the design process. For the Z-stage, which have a significantly higher resonant mode than that of X and Y stages, analysis was performed by constraining the X and Y stages to avoid unnecessary computational efforts. Material properties used in these analyses are documented in Table 1.

Fig. 2 shows the results of the modal analysis of the scanner assembly. The first resonant mode is along the actuation direction of Y-stage at 7.67 kHz, and the second resonance frequency is the rocking mode of the X-stage at 10.26 kHz. The third mode is along the actuation direction of the X-stage at 16.4 kHz. The resonant mode along the Z-actuation is seen at 115.4 kHz.

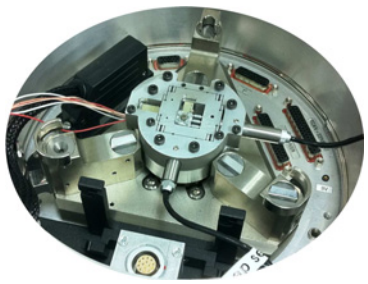

Figure 4 *Scanner assembled inside the commercial NT-MDT NTEGRA scanning probe microscope*

4. Frequency response: To study the dynamic characteristics of the scanner, a HP35670A dual-channel spectrum analyser was used to measure the frequency response in x and y directions. A Polytec PSV-Z-040 single-point laser vibrometer was used to measure the frequency response along the z-direction, since the measurement bandwidth of the spectrum analyser was limited to 50 kHz, which is below the Z-stage resonance predicted by FEA.

Input signals from HP35670A spectrum analyser, in the form of a swept sine, having amplitude of 50 mVpk, in a frequency range of 10 Hz to 20 kHz, are applied through the PiezoDrive amplifiers, to drive the piezoelectric stack actuators in the x and y directions. In the case of z-direction, input signals from laser vibrometer controller, in the form of a swept sine, having amplitude of 50 mVpk, in a frequency range of 1–100 kHz, are applied through the PiezoDrive amplifiers, to drive the actuator. Capacitive sensors are used to measure the displacement in volts. Fig. 3 shows the plots of the frequency response along the three directions. For the Y-stage, resonant modes can be seen in the form of peaks at 4 and 7 kHz in the magnitude response. In the case of the X-stage, the resonant peak appears at 10 kHz. The first resonant peak of the Z-stage is observed at 64 kHz.

It is evident that there are discrepancies between FEA and experimentally obtained frequency response of the system. From the FEA, the prominent mode is seen at 7.67 kHz along the actuation direction for the Y-stage. In the measured frequency response, another mode at 4 kHz can be seen before the actuation mode at 7 kHz. Preliminary investigations revealed that the mechanism used to pre-load the piezoelectric stack actuator acts like a soft

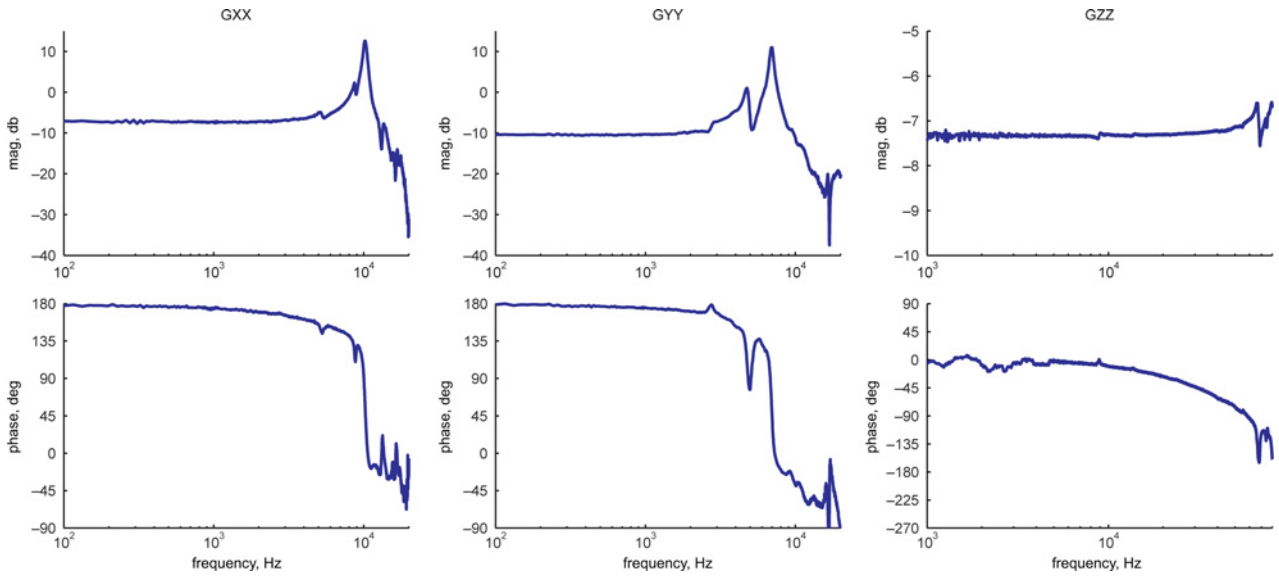

Figure 3 *Frequency response of the scanner along x, y and z-directions*

spring on the system. This reduces the resonance frequency to 4 kHz. In the case of the X-stage, the first resonant peak is seen at 10 kHz in the frequency response which is the rocking mode as predicted by FEA. For the Z-stage, the amplifier bandwidth was insufficient. Consequently, a significant drop in phase was observed in the frequency response. The bandwidth of the amplifier, for a load capacitance $C = 35$ nF, was calculated to be 150 kHz from (7) below [14], which explains the drop in phase from 150 Hz:

$$f^{3\,\mathrm{dB}} = \frac{1}{190C}\,\mathrm{Hz} \tag{7}$$

5. Scanner imaging capability: To evaluate the imaging capability of the scanner, it was installed in a NT-MDT NTEGRA SPM (see Fig. 3) and was used to obtain images of a MikroMasch TGQ01 calibration grating. The grating has parallel step features of 3 μm period and 20 nm height. Images of 6 × 4.5 μm scan size with pixel resolution of 256 × 256 were recorded at 10, 50, 78, 100, 120 and 150 Hz. Further increase in speed was restricted by the limitation of the Z-feedback bandwidth [15] and data acquisition system. Fig. 4 shows the images recorded at 10, 50, 78, 100, 120 and 150 Hz. A close observation reveals that the width of the feature is not identical due to the presence of hysteresis. The limitation of the Z-feedback bandwidth is evident from the rounded corners of the features in images obtained at high speed. Fig. 5*p* clearly shows the presence of hysteresis due to piezoelectric stack actuators. Hysteresis loop was measured for the lateral axis and was presented in [16]. It was found that the width of the loop is 29% of the full range along the *X*-axis and 31% along the *Y*-axis.

It can be observed in Fig. 5*p* that vibrations start to appear at 100 Hz. Note that rastering involves actuation of the fast stage with triangular signals. A triangular signal has odd harmonics of

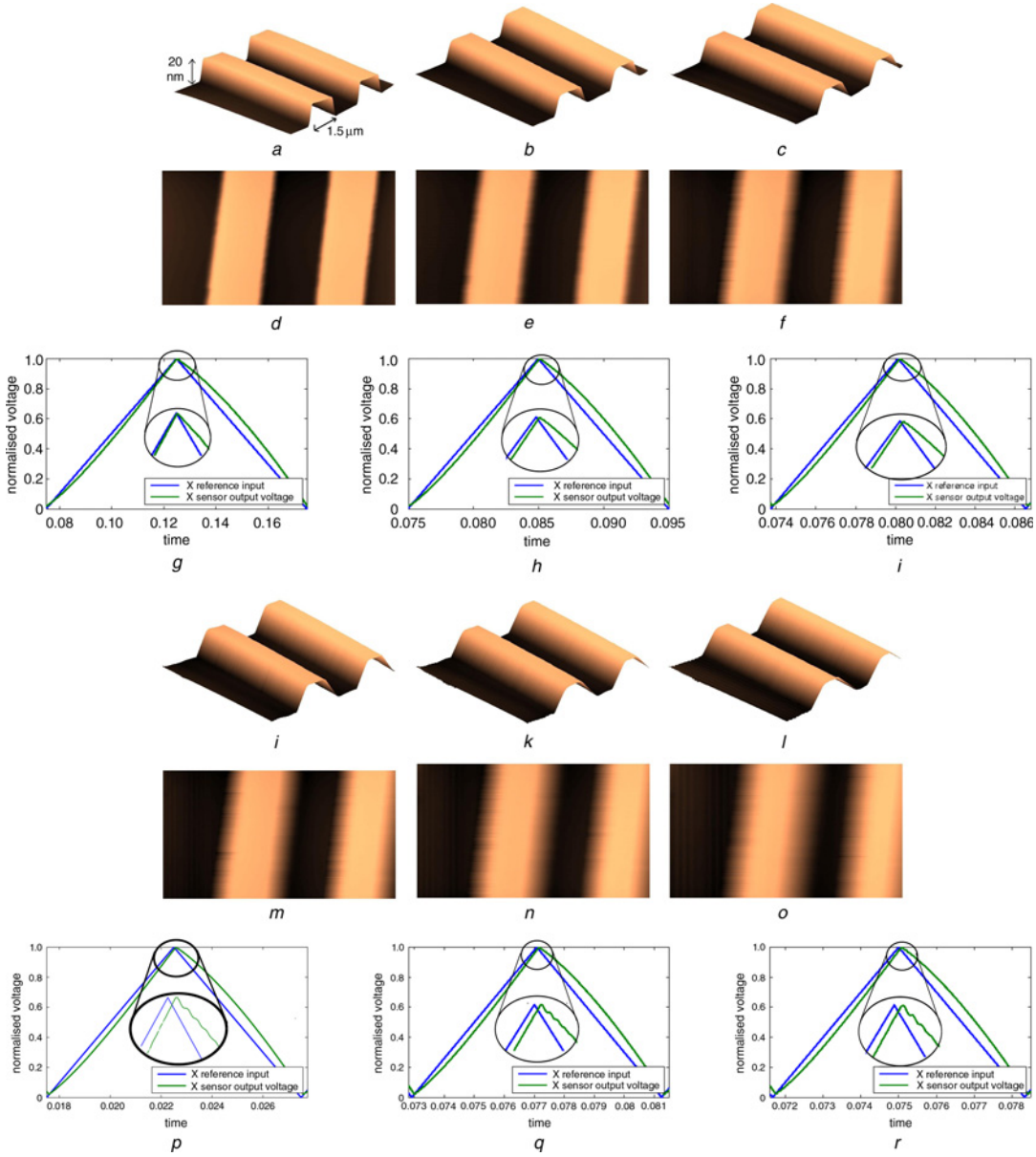

Figure 5 *Open-loop scan performance of the scanner with lines rates*
a, *d*, *g* 10 Hz
b, *e*, *h* 50 Hz
c, *f*, *i* 78 Hz
j, *m*, *p* 100 Hz
k, *n*, *q* 120 Hz
l, *o*, *r* 150 Hz

doi: 10.1049/mnl.2011.0477

its fundamental frequency which interact with the resonant modes of the structure causing artefacts in the images. This interaction of harmonics restricts the scanning rate to 1/100th of the resonance frequency [17]. The resonance for fast stage appears at around 10 kHz, which means the maximum scan speed is limited to around 100 Hz, as is evident in Fig. 5*p*.

Scans were performed using the standard controller for the vertical axis available from the commercial AFM. This controller is customised for low-speed scanning using the piezoelectric tube scanner and has low bandwidth. While performing high-speed scans, distortions such as rounding of sharp edges and slanting of the vertical features can be observed. These are anomalies and can be distinctly seen in Figs. 5*p*–*r*.

Thus, three of the main causes for degradation of images are (i) interaction of harmonics of fundamental frequency of input signals with the resonance frequency of the stage causing oscillations to appear in the images, (ii) nonlinear effects due to hysteretic behaviour of piezoelectric causing discrepancies in the features and (iii) insufficient vertical bandwidth causing the rounding of sharp edges of the features.

6. Conclusions and future work: This Letter presented a systematic procedure for designing a high-speed, compact serial-kinematic scanner for high-speed AFM. The analytical, FEA and experimental results were presented. It is seen that for the X-stage the analytical estimation does not produce the desired results. The rocking is seen at the first mode while the mode along the actuation direction is the second mode. Hence, the X-stage cannot be considered as a SDOF system along the actuation direction. For the Y-stage analytical estimate, FEA and experimental results were in agreement. The anomalies in the FEA and experimental results were due to the preloading mechanism. The preloading mechanism will be improved in near future. The scanner was installed in a commercial AFM to check the performance of the scanner. Oscillations were seen around 100 Hz while the presence of hysteresis was also observed. Scanned images of a calibration sample in open loop, up to scan frequency of 150 Hz, were acquired and presented. Future work includes improving the out-of-plane stiffness of the X-stage, developing proper preloading technique for piezoelectric actuators and exploring suitable control algorithm [18] for the stage to enhance its performance.

7 References

[1] Binnig C.F., Quate G.: 'Atomic force microscope', *Phys. Rev. Lett.*, 1986, **56**, pp. 930–933

[2] Ando T., Uchihashi T., Kodera N., *ET AL.*: 'High-speed AFM and nano-visualization of biomolecular processes', *Pflgers Arch. Eur. J. Physiol.*, 2008, **456**, pp. 211–225

[3] Schitter G., Astrom K., DeMartini B., Thurner P., Turner K., Hansma P.: 'Design and modeling of a high-speed AFM scanner', *IEEE Trans. Control Syst. Technol.*, 2007, **15**, (5), pp. 906–915

[4] Devasia S., Eleftheriou E., Moheimani S.O.R.: 'A survey of control issues in nanopositioning', *IEEE Trans. Control Syst. Technol.*, 2007, **15**, (5), pp. 802–823

[5] Schitter G., Rost M.J.: 'Scanning probe microscopy at video-rate', *Mater. Today*, 2008, **11**, (Supplement 1), pp. 40–48

[6] Kindt J.H., Fantner G.E., Cutroni J.A., Hansma P.K.: 'Rigid design of fast scanning probe microscopes using finite element analysis', *Ultramicroscopy*, 2004, **100**, (3–4), pp. 259–265

[7] Yong Y.K., Lu T.-F., Handley D.C.: 'Review of circular flexure hinge design equations and derivation of empirical formulations', *Precision Eng.*, 2008, **32**, (2), pp. 63–70

[8] Paros J., Weisbord L.: 'How to design flexure hinge', *Mach. Des.*, 1965, **37**, pp. 151–156

[9] Lobontiu N., Paine J.S.N., Garcia E., Goldfarb M.: 'Corner-filleted flexure hinges', *J. Mech. Des.*, 2001, **123**, (3), pp. 346–352

[10] Yong Y.K., Lu T.: 'The effect of the accuracies of flexure hinge equations on the output compliances of planar micro-motion stages', *Mech. Mach. Theory*, 2008, **43**, (3), pp. 347–363

[11] Kenton B.J., Leang K.K.: 'Design and control of a three-axis serial-kinematic high-bandwidth nanopositioner', *IEEE/ASME Trans. Mechatron.*, 2011, **PP**, (99), pp. 1–14

[12] Timoshenko S., Goodier J.: 'Theory of elasticity' (McGraw-Hill, 1970, 3rd edn.)

[13] Yong Y.K., Aphale S.S., Moheimani S.O.R.: 'Design, identification and control of a flexure-based XY stage for fast nanoscale positioning', *IEEE Trans. Nanotechnol.*, 2009, **8**, (1), pp. 46–54

[14] PiezoDrive.: 'PDL 200 piezodrive specifications'

[15] Fleming A.J.: 'Dual-stage vertical feedback for high speed scanning probe microscopy', *IEEE Trans. Control Syst. Technol.*, 2011, **19**, (1), pp. 156–165

[16] Wadikhaye S., Yong Y.K., Moheimani S.O.R.: 'A novel serial-kinematic AFM scanner: design and characterization'. Proc. 37th Annual Conf. IEEE Industrial Electronics Society (IECON 2011), 7–10 November 2011

[17] Aphale S.S., Fleming A.J., Moheimani S.O.R.: 'High speed nano-scale positioning using a piezoelectric tube actuator with active shunt control', *Micro Nano Lett.*, 2007, **2**, (1), pp. 9–12

[18] Aphale S.S., Bhikkaji B., Moheimani S.O.R.: 'Minimizing scanning errors in piezoelectric stack-actuated nanopositioning platforms', *IEEE Trans. Nanotechnol.*, 2008, **7**, (1), pp. 79–90